Experimental Investigation of a Johnson Noise Thermometry Using GMR Sensor for Electric Vehicle Applications

Xuyang Liu, *Student Member, IEEE*, Chao Zheng, Chunhua Liu, *Senior Member, IEEE*, and Philip W. T. Pong, *Senior Member, IEEE*

***Abstract*— A new temperature measurement method using a giant magnetoresistance (GMR) sensor based on Johnson noise thermometry (JNT) is proposed in this paper. This paper presents the principle of this GMR-based JNT and demonstrates its feasibility by measuring power spectral density of noise voltage in the bandwidth from 10 kHz to 22.8 kHz and resistance of GMR sensor and analyzing their relationship with the absolute temperature. The measuring errors throughout the measurement of temperature from −40 °C and 150 °C in the thermal chamber were less than ±1.8 °C with integration time of 58.6 s. Its dynamic sensing performance under both varying temperature and changing external magnetic field was characterized and demonstrated. A practical demonstration of the GMR-based JNT for measurement of surface temperature of a battery pack on an electric-vehicle testbed was also provided. Therefore, it is feasible to implement this new thermometry with a GMR sensor, making spintronic sensor multifunctional in EV applications by being a temperature sensor as well.**

***Index Terms*— Johnson noise thermometry (JNT), GMR sensor, electric vehicle, multifunctional spintronic sensor.**

I. Introduction

TEMPERATURE monitoring of the energy storage system and traction system in electric vehicles (EVs) plays a major role in ensuring an EV's safety, reliability, and efficiency. The battery temperature affects many physical processes in EV batteries. For example, the internal resistance of a battery typically falls with increasing temperature, and high battery temperature can shorten the lifespan of EV batteries. The typical optimum operating temperature for EV battery is in the range of 30 ∼ 40 °C [1]. Overheating during battery charging and operation is one major factor that leads to the malfunction of an EV [2], [3]. The reliable measurement and management of battery temperatures can avoid overheating issues, ensuring the safety of an EV and maximizing the lifetime of EV batteries. On the other hand, traction motor also needs the reliable temperature monitoring. Exceeding the rated temperature by 10 °C significantly reduces the lifetime of a three-phase induction motor by 50% [4]. Overheating also causes the permanent magnets in motors to lose effectiveness and strength. An electric motor needs to avoid operating at temperature over 125 °C in order to fully utilize its potential [5]. Hence, accurate and reliable temperature measurement for EV batteries and motors is of the essence in EVs.

Thermocouple and resistance thermometer are the most frequently used temperature measurement techniques in EV applications [6]–[8]. Mechanism of thermocouple is based on the Seebeck effect, which describes an electromotive force that is proportional to the temperature difference between two junctions of dissimilar conductors [9]; whilst a resistance thermometer directly relates the temperature to the resistance of a conductive material. However, the outputs of thermocouple and resistance thermometer always drift due to the environmental effects (*e.g.*, high temperature, high pressure, oxidation, corrosion, vibration) [10]. Periodic recalibration and eventual replacement of a thermocouple or resistance thermometer are required to ensure accurate temperature readings. Hence, thermocouples and resistance thermometers are undesirable for the long-term reliable temperature measurement in EV applications.

Johnson noise thermometry (JNT) is a method capable of accurate evaluation of the thermodynamic temperature [11]. In recent years, considerable progress has been made in JNT by improvements in sensing methods and modern electronic technologies. By using a temperature-dependent diode as a temperature sensor, fast JNT was achieved with accuracies in the order of a small fraction of 1 K in the temperature range from 300 to 400 K [12]. A combined thermocouple-noise temperature sensor at temperatures above 1000 °C was successfully investigated with relative measurement uncertainties of about 0.1% [13]. Through high frequency and wide bandwidth JNT, a precision of 0.01% has been achieved on auto- and cross-correlated noise measurements with integration time of 1s [14]. Meanwhile, the accuracy of JNT has also been

Manuscript received January 25, 2018; accepted February 6, 2018. Date of publication February 12, 2018; date of current version March 22, 2018. This work was supported in part by the Seed Funding Program for Basic Research, in part by the Seed Funding Program for Applied Research and Small Project Funding Program from the University of Hong Kong, in part by ITF Tier 3 funding under Grant ITS/203/14, Grant ITS/104/13, and Grant ITS/214/14, in part by RGC-GRF under Grant HKU 17210014 and Grant HKU 17204617, and in part by the University Grants Committee of Hong Kong under Grant AoE/P-04/08. The associate editor coordinating the review of this paper and approving it for publication was Dr. Cheng-Ta Chiang. *(Corresponding author: Philip W. T. Pong.)*

X. Liu, C. Zheng, and P. W. T. Pong are with the Department of Electrical and Electronic Engineering, University of Hong Kong, Hong Kong (e-mail: liuxy@eee.hku.hk; stevenzc@connect.hku.hk; ppong@eee.hku.hk).

C. Liu is with the School of Energy and Environment, City University of Hong Kong, Hong Kong (e-mail: chualiu@eee.hku.hk).

Digital Object Identifier 10.1109/JSEN.2018.2805309

significantly improved by the recent development of quantum voltage noise source (QVNS) [15], [16].

Due to multiple unique features such as high sensitivity, low cost, compactness, low energy consumption and compatibility with standard CMOS technologies, giant magnetoresistance (GMR) sensors are promising for large-scale industrial applications [17]–[26], such as EVs. Recent research has also investigated a number of different GMR effects and related materials in an attempt to enhance GMR sensors in various sensing applications [27]–[30]. Both parameters of temperature and magnetic field are needed to be monitored in an EV. Temperature monitoring of energy storage system and traction system is critical in ensuring an EV's safety, reliability, and efficiency. GMR sensors are already widely applied in EVs and automotive applications for measurement of the rotation angle or speed of motors and wheels by detecting the magnetic field variation [17]–[21]. GMR sensors are also capable of sensing the driving current of motors and the charging/discharging current of EV batteries in a non-contact way [22]–[25], [31]. Therefore, it is promising to develop a multifunctional magnetoresistive sensor in EV applications, which is capable of measuring velocity, current as well as temperature in one sensor.

This paper presents a novel Johnson noise thermometry (JNT) using a GMR sensor as a temperature transducer, which provides high linearity and high noise immunity in a wide temperature range from −40 °C to 150 °C. This GMR-based JNT operating under both constant and varing external magnetic fields was experimentally studied, and the temperature can be accurately determined from the Johnson thermal noise and sensor resistance. This proposed GMR-based JNT makes the GMR sensor multifunctional for EV applications, which enables the dual-parameter measurement of magnetic field and temperature using a sensor. Such a multifunctional sensor can significantly reduce the complexity of sensing circuit system and thus the overall construction costs of an EV. Moreover, the GMR-based JNT is not as vulnerable to the harsh environment, material degradation or periodic recalibration as the above-mentioned temperature sensors, and thus it can be a promising substitute for measuring temperature in EV applications.

This paper is organized as follows. Section II provides the fundamental principle of the GMR-based JNT, whilst Section III describes the experimental design for the proposed JNT using a GMR sensor. Section IV shows the experimental results verifying the feasibility and accuracy of the proposed approach. Section V demonstrates the practical test of the GMR-based JNT for battery pack during operation. Section VI addresses the conclusions and outlook of this work.

II. Operating Principle of GMR-Based JNT

Johnson noise thermometry measures both the resistance of a conductor and its inherent thermal noise (also known as Johnson noise) for determining the absolute temperature. Johnson noise pervasively appears in all types of conducting media due to the random motions of charge carriers agitated by local temperature variations near Femi level [11], [32]. In theory, Johnson noise voltage across an ideal resistor exhibits a flat (white) spectral energy distribution that does not depend on the frequency (except at extremely high frequency). For frequency below a few gigahertz, the power spectral density (PSD) of the Johnson noise voltage across a conductor is expressed by the Johnson-Nyquist equation [13] as below:

$$\begin{aligned} S_{vT} &= 4k_B T_{(K)}(R_0 + R(T_{(K)})) \\ &= 4k_B T_{(K)} R_{cut} \end{aligned} \tag{1}$$

where S_{vT} denotes the theoretical PSD value of Johnson noise voltage, k_B is the Boltzmann's constant (1.3806×10^{-23} J/K), $T_{(K)}$ is the absolute temperature in Kelvin (K), and R_{cut} is the resistance of the conductor under test which contains both the temperature-independent component (R_0) and the temperature-dependent component ($R(T_{(K)})$).

In practice, there exists an overall offset (S_{bg}) between the actually measured noise PSD (S_v) and the theoretical noise PSD value (S_{vT}) due to the background noise floor from the measuring system. Thus, Eq. (1) can be modified as:

$$S_v = S_{bg} + S_{vT} = S_{bg} + 4k_B T_{(K)} R_{cut} \tag{2}$$

The background noise floor may be caused by the intrinsic noises of preamplifiers, external electromagnetic interferences and transmission error [13], [33], and its value can be determined by the pre-calibration before the actual measurements.

Since S_v, S_{bg} and R_{cut} can be measured, $T_{(K)}$ can be derived from Eq. (3) as below:

$$T_{(k)} = \frac{S_v - S_{bg}}{4k_B R_{cut}} \tag{3}$$

No recalibration is required for JNT, as the relation among temperature, noise PSD and resistance is intrinsic and JNT is independent of any material degradation [24]. The structural and material properties of the sensing conductor change with time due to harsh environmental effects (*e.g.*, oxidation, corrosion, vibration, *etc*.), which gradually results in the variation of the conductor resistance (R_{cut}). According to the Johnson-Nyquist theorem, thermal noise PSD (S_v) is dependent of R_{cut} and T, leading to the fact that both S_v and R_{cut} may drift due to the environmental effects over time. However, for JNT, the absolute temperature is determined by the concurrent measurement of both thermal noise PSD and sensor resistance, so effects of harsh environment on temperature measurement are already considered and included in the calculation. Therefore, JNT is especially suitable for harsh industrial environment such as nuclear reactors [11], where the materials of the sensing devices may significantly degrade with time.

In this work, a new JNT using a GMR sensor as the sensing resistor is proposed. GMR sensors normally function as magnetic field sensors with their resistance (R_{gmr}) varying with external magnetic field (H) and temperature ($T_{(K)}$), which can be described by $R_{gmr} = R_0 + R(H) + R(T_{(K)})$. Thus the thermal noise PSD (S_v) of GMR sensors is dependent on both H and $T_{(K)}$. To implement JNT with a GMR sensor, R_{cut} in Eq. (3) can be replaced with R_{gmr}. Similar to the traditional JNT, the relation among R_{gmr}, S_v and $T_{(K)}$ is

governed by Eq.(4):

$$T_{(k)} = \frac{S_v - S_{bg}}{4k_B R_{gmr}} \tag{4}$$

This relation still holds even when both temperature and magnetic field vary at the same time, and there is no need to differentiate resistance change due to temperature or magnetic field. Hence, $T_{(K)}$ can be determined accordingly by the measuring R_{gmr} and S_v of a GMR sensor. The influence of the external field on the noise PSD and thus the GMR-based JNT temperature measurement is already handled by the fact that the resistance of the GMR sensor is being measured continuously. As such, the measurement of temperature by the GMR-based JNT through Eq. (4) can be independent of the external magnetic field. The magnetic parameters (*e.g.*, resolution, field-sensitivity, *etc.*) of a GMR sensor do not affect its JNT temperature measurement results. Thus the GMR-based JNT can still operate even when the GMR sensor experiences external magnetic field.

III. Experimental Preparation

A. GMR Sensor Model

A bipolar GMR sensor model (Sensitec GF708) was selected to investigate and implement the GMR-based JNT. Other GMR sensors besides GF708 or even tunnelling magnetoresistive (TMR) sensors are also applicable for this approach. GMR sensors generally show higher temperature-sensitivity regarding JNT behaviors than TMR sensors due to their higher temperature coefficient of resistance (TCR) [34]–[36]. The GF708 sensor model offers a sensitivity of typically 130 mV/V/mT to magnetic field, and is frequently used for sensing magnetic field in various kinds of applications [37]–[39]. The GF708 sensor consists of four spin-valve elements arranged in a Wheatstone bridge configuration, as illustrated in Fig. 1. Two spin-valve elements (R_2 and R_4) are covered by the flux concentrators (shields) to prevent the applied magnetic field influencing them, while the other two elements (R_1 and R_3) change in resistance when an external field is applied [40]. Usage of Permalloy flux concentrators (shields) also leads to the introduction of undesirable effects such as additional magnetic noise perturbations and hysteresis effect [41]. In the GMR-based JNT, no bias voltage supply was applied across the pads Vcc and GND of the Wheatstone bridge in order to eliminate other noise sources besides Johnson noise (see Fig. 1). Bridge resistance between pads A and B was measured as the resistance of GMR sensor (R_{gmr}).

The resistance (R_{gmr}) of the GMR sensor across the Wheatstone bridge needs to be monitored continuously in the GMR-based JNT as explained in Section II. A typical resistance-field transfer curve for the resistance (R_{gmr}) of the GF708 GMR sensor was obtained experimentally by applying magnetic field along the sensitive axis as shown in Fig. 2. R_{gmr} depends on both the external magnetic field and temperature. It varies significantly in the range approximately from −2.0 Oe to 3.6 Oe, and it saturates when the magnitude of the applied field exceeds this range. The hysteresis of the GMR sensor is clearly visible in Fig. 2. R_{gmr} also increases with temperature

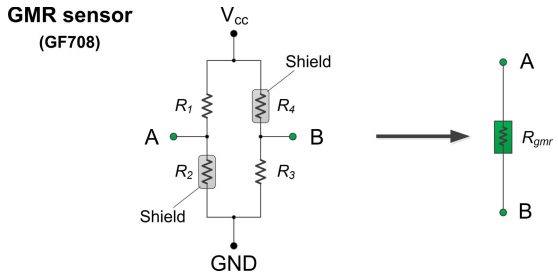

Fig. 1. Circuit diagram of GMR sensor GF708. No bias voltage supply was applied across the pads Vcc and GND of the Wheatstone bridge in order to eliminate other noise sources besides Johnson noise. Bridge resistance between pads A and B was measured as the resistance of GMR sensor (R_{gmr}).

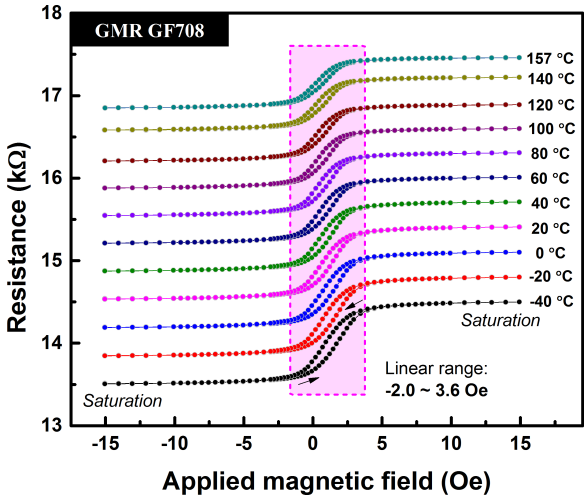

Fig. 2. Typical characteristic resistance-field transfer curves of the GMR sensor GF708.

in general. Meanwhile, the characteristics curve also indicates that GMR sensor GF708 can function up to nearly 160 °C.

B. Experimental Setup

Experiments were carried out to investigate the feasibility and accuracy of the GMR-based JNT. The schematic of the experimental setup is illustrated in Fig. 3. A GMR sensor GF708 was placed inside a thermal chamber (ESPEC SH242). Temperature inside the thermal chamber can be controlled in the range from −40 °C to 160 °C with temperature stability of 0.5 °C. A K-type thermocouple and a Platinum resistance thermometer (PRT) were placed in close proximity to the GMR sensor in order to provide reference temperatures for comparison with the temperature obtained by the GMR-based JNT. The temperature readings of the thermocouple were collected by a thermocouple input module (NI USB-TC01). To provide a uniform external magnetic field parallel to the sensitive axis of the GMR sensor, a programmable bipolar power supply (KIKUSUI PBZ40-10) was used to power a single-axis Helmholtz coil of radius 40 mm. The Helmholtz coil was also placed in the thermal chamber with the GMR sensor placed at its centre. The magnetic field generated by the Helmholtz coil was calibrated against the coil current using a DSP Gaussmeter (Lakeshore model 455). The Helmholtz coil

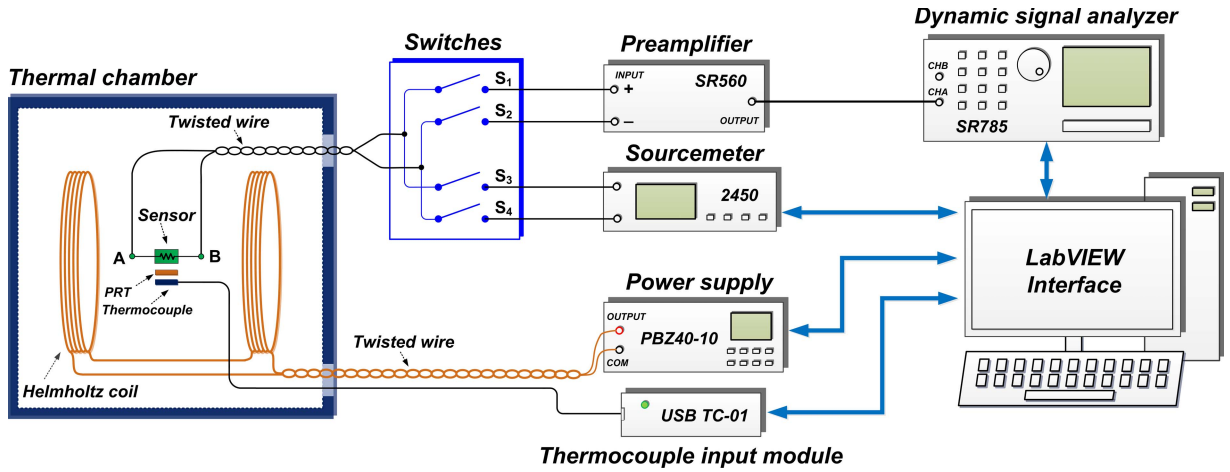

Fig. 3. Schematic diagram of the experimental setup for the GMR-based JNT.

was then powered at constant current mode inside the chamber so that the coil current and thus magnetic field generated remained stable even when the chamber temperature varied. As the charging/discharging current flowing through the DC link connecting to the battery pack in an EV can reach to 50 A or higher [42], the DC link can generate a magnetic field up to 15 Oe at its near surface (e.g. at a distance of 2 mm). Hence, the largest magnitude of the Helmholtz-coil magnetic field was applied as 15 Oe in this study.

The open-circuit noise voltage across the GMR sensor was amplified 1000 times by a low-noise, AC-coupled differential voltage preamplifier (SRS SR560). Twisted wires were also used to suppress the coupling noise. A dynamic signal analyzer (SRS SR785) was employed to measure the amplified noise signal and perform the fast Fourier transform calculations for obtaining the power spectrum. The resistance (R_{gmr}) of the GMR sensor across the Wheatstone bridge was continuously monitored by a source-meter (Keithley 2450). The measurement system can choose to measure the noise PSD (S_v) or resistance of GMR sensor (R_{gmr}) by means of switches. When S_1 and S_2 were switched on (S_3 and S_4 were switched off), the GMR sensor was connected to the preamplifier directly and the noise PSD was measured. When S_3 and S_4 were switched on (S_1 and S_2 were switched off), the resistance of the GMR sensor was measured. All the above-mentioned instruments were controlled and automated through the LabVIEW program which can also collect and process the measured data to determine the temperature.

The power spectrum of noise voltage was firstly observed in the frequency bandwidth between 10 Hz and 102.4 kHz, and its typical power spectrum after 1000 times averaging is depicted in Fig. 4(a). It shows that the frequency-dependent 1/f noises of structural and magnetic origin existing in GMR sensor are much larger than the Johnson noise at frequencies below 1 kHz, and it is not influenced by the temperature. The observation bandwidth should be large enough to avoid 1/f noise fluctuations. The three peaks (i.e. 50 Hz, 150 Hz and 250 Hz) in the low-frequency range were due to the power supply frequency and its harmonics. The mid-frequency noise spectrum (i.e. approximately from 5 kHz to 30 kHz) demonstrates the flat frequency-independent characteristic of

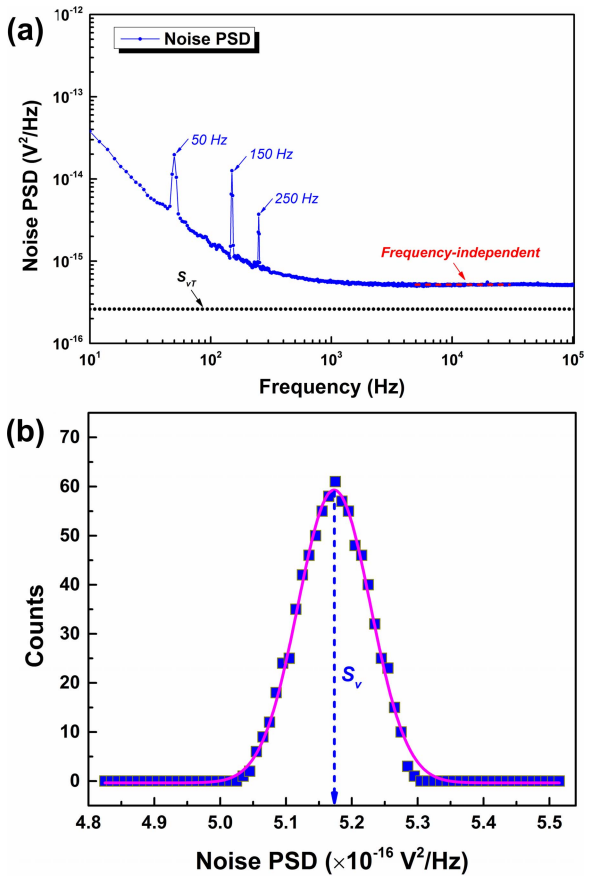

Fig. 4. (a) The power spectrum of the noise voltage in the bandwidth from 10 Hz to 102.4 kHz. (b) Gaussian fitting of the histogram of the noise spectrum from 10 kHz to 22.8 kHz to determine noise PSD value.

Johnson noise (see the red dotted line in Fig. 4(a)). Therefore, the observation bandwidth starting from 10.0 kHz to 22.8 kHz is high enough to avoid 1/f noise fluctuation, which was chosen for determination of noise PSD values.

During the noise measurement, the noise spectrum between 10.0 kHz and 22.8 kHz was averaged 1000 times, which cost an integration time of approximately 58.6 seconds. To estimate the amplitude of this frequency-independent noise, histogram analysis between 10.0 kHz and 22.8 kHz (800 FFT points) of the spectrum was performed as shown in Fig. 4(b). The

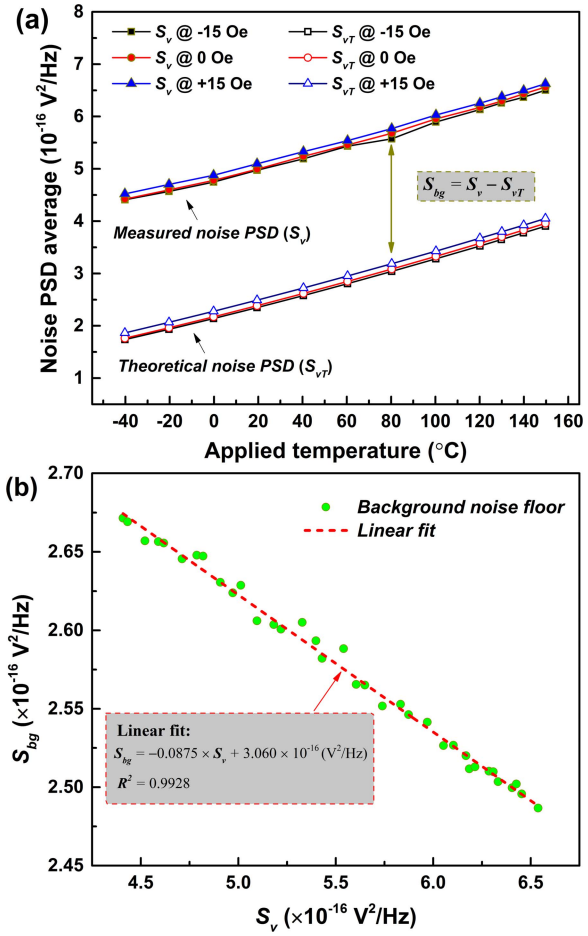

Fig. 5. (a) Comparison between the measured noise PSD (S_v) and the theoretical noise PSD values (S_{vT}). (b) A linear fit of the background noise floor (S_{bg}) versus measured noise PSD (S_v).

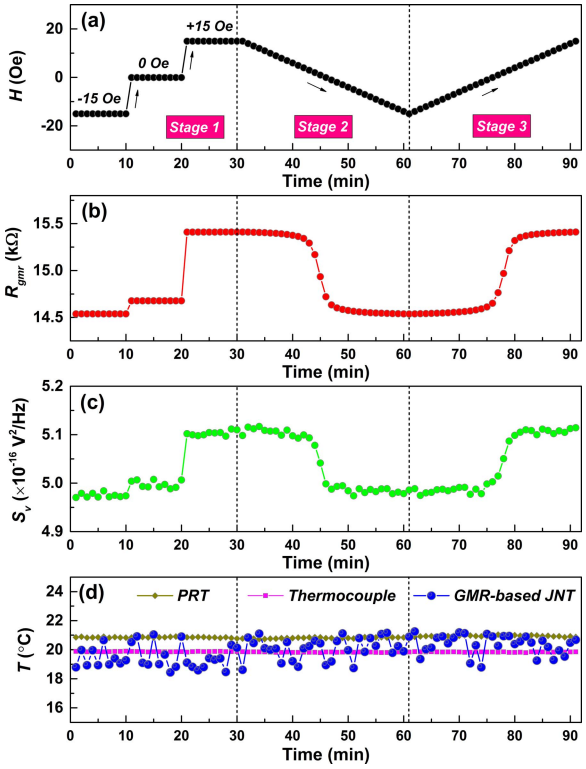

Fig. 6. Temperature measurement by the GMR-based JNT at approximately 20 °C with constant and variable magnetic fields applied.

mean value (i.e. where the peak occurs) of the Gaussian fit of the obtained histograms provides a more reasonable representation of the average noise power than just the average of the PSD spectrum, because the sporadic sharp sparks (e.g. due to EMI) which exhibit very few occurrence in the spectrum (i.e. low counts in histogram) and do not affect much the peak position of Gaussian fitting. This technique for determining the amplitude of noise PSD has also been applied by other groups in their scientific analysis [43]–[45].

C. Determination of Background Noise Floor

The pre-calibration process involves providing the background noise floor of the measuring system. In the pre-calibration process, averaged noise PSD values (S_v) across the GMR sensor were measured at temperatures ranging from −40 °C to 150 °C under the applied magnetic fields of −15 Oe, 0 Oe and +15 Oe, respectively, then these measured values were compared with the theoretical noise PSD values (S_{vT}) at each testing condition, as illustrated in Fig. 5(a). It can be observed that there exists an overall offset (S_{bg}) between the measured noise PSD and the theoretical values, which is the background noise floor of this measuring system, and it may result from the parasitic noise signals of preamplifier, leads and switches, the preamplifier gain frequency dependence, etc. The noise PSD offset (S_{bg}) decreases linearly with the rise of the measured noise PSD (S_v), as shown in Fig. 5(b). A linear fit of the noise PSD offset (S_{bg}) versus the measured noise PSD (S_v) was carried out (see red dash line in Fig. 5(b)) to determine the background noise floor, which can be expressed as follows:

$$S_{bg} = -0.0875 \times S_v + 3.06 \times 10^{16} \ (\mathrm{V^2/Hz}) \qquad (5)$$

Substituting (5) into (4), the relation among the temperatures in °C ($T_{(°C)}$), measured noise PSD (S_v) and measured resistance (R_{gmr}) of GMR sensor can be established as follows:

$$T_{(°C)} = \frac{-1.0875 \times S_v - 3.06 \times 10^{16}}{4k_B R_{gmr}} - 273.15\mathrm{K} \qquad (6)$$

IV. Experimental Result

The investigation was firstly conducted to check whether external magnetic field would affect the GMR-based JNT. The temperature inside thermal chamber was set to remain constant at 20 °C. An external magnetic field (H) was applied parallel to the sensitive axis of the GMR sensor in three stages (see Fig. 6(a)). During Stage 1, the applied magnetic field was changed from −15 Oe to 0 Oe (i.e. with no magnetic field applied) and finally to +15 Oe. During Stage 2, the applied field gradually swept from +15 Oe to −15 Oe. During Stage 3, the applied filed gradually increased from −15 Oe to +15 Oe. As we can see from Fig. 6(b), the resistance (R_{gmr}) of GMR sensor varied with the applied field according to its

characteristic resistance-field transfer curve as characterized in Fig. 2. The averaged noise PSD (S_v) varied similarly as R_{gmr} (see Fig. 6 (c)) because they are related by Eq. 4. During these three Stages, the temperature ($T_{(°C)}$) were determined through Eq. 6 using the measured R_{gmr} and S_v, and then compared with the reference temperature obtained by the thermocouple and the PRT, as shown in Fig. 6(d). The reference temperatures obtained by the thermocouple and the PRT were nearly constant at ~19.81 °C (with a variation of ~0.09 °C) and ~20.86 °C (with a variation of ~0.31 °C), respectively. The absolute measuring error (ΔT) between the temperature ($T_{(°C)}$) measured by GMR-based JNT and the reference temperature is rather small (within the range of $-1.42 \sim +1.76$ °C). Despite the variation of R_{gmr} due to the applied field, $T_{(°C)}$ closely matched with the reference temperatures and it was not affected by the applied field. The experimental results also demonstrated that the GMR-based JNT can still operate even the GMR sensor is saturated by large field such as −15 Oe and +15 Oe. The saturation states of the GMR sensor nearly do not affect the temperature measurement results by the GMR-based JNT. Moreover, it also should be noted that the hysteresis of GMR sensor does not affect the performance of the GMR-based JNT.

The performance of the GMR-based JNT over a wide temperature range was studied. The temperature of the thermal chamber (i.e. the applied temperature) was varied from −40 °C to 150 °C, while the R_{gmr} and S_v were measured under the applied field of −15 Oe, 0 Oe and 15 Oe respectively at each temperature set point (see Fig. 7(a) and Fig. 7(b)). R_{gmr} increased linearly with the rise in temperature. S_v also increased with the temperature because S_v is related to R_{gmr} as defined by Eq. (4). Fig. 7(c) shows the temperature ($T_{(°C)}$) determined by Eq. (6) using the measured R_{gmr} and S_v, whilst Fig. 7(d) shows the measuring error (ΔT) comparing to the reference temperature obtained from the thermocouple. The measured temperatures under three applied fields closely matched with the reference temperatures. The measuring error ΔT was in the range between −0.95 °C and 1.47 °C. Meanwhile, the GMR-based JNT also demonstrated a good linearity in the measurement range from −40 °C to 150 °C. Moreover, the GMR-based JNT using the GMR sensor GF708 was experimentally verified to be capable of operating in a wide temperature range from −40 °C to 150 °C with a measuring error of less than ±1.5 °C. The measuring error of the GMR-based JNT can be further reduced by optimizing the performance of preamplifiers, pre-calibration techniques and data processing algorithms.

The dynamic performance of the GMR-based JNT was also studied and characterized. In this experiment, an external magnetic field was applied to the GMR sensor in three stages, as shown in Fig. 8(a). During Stage 1, the applied field varied from −15 Oe to 0 Oe and finally to +15 Oe. During Stage 2, the applied filed first gradually swept from +15 Oe to −15 Oe, and then reversely swept from −15 Oe to +15 Oe. During Stage 3, the applied field was changed from +15 Oe to 0 Oe, and then to −15 Oe. In the meanwhile, a temperature cycle between 30 °C and 90 °C inside the thermal chamber was provided. The temperature inside the thermal chamber was first

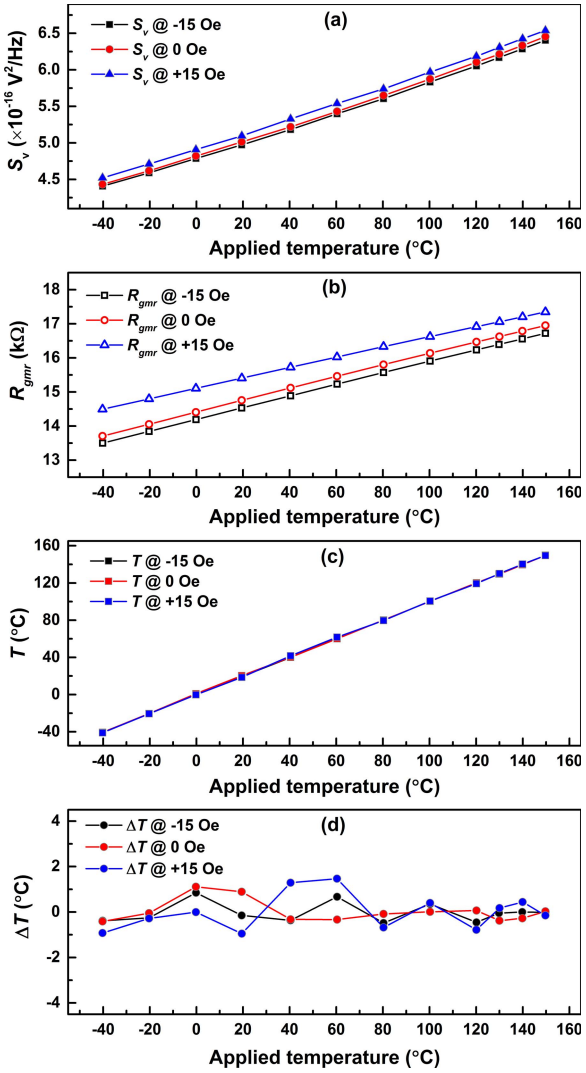

Fig. 7. Temperature measurement in the range from −40 °C to 150 °C: (a) averaged noise PSD (S_v); (b) sensor resistances (R_{gmr}); (c) temperature results (T); and (d) measuring errors (ΔT).

stabilized at 30 °C for approximately 30 minutes, and then it gradually increased to 90 °C and remained stable at 90 °C for approximately 30 minutes. Finally it decreased to 30 °C and finally remained stable at 30 °C. The R_{gmr} and S_v responded in the same manner to the variation of temperature and applied magnetic field, as shown in Fig. 8(b) and Fig. 8(c) respectively. The temperature measured by the GMR-based JNT closely matched with the reference temperatures measured by the PRT and thermocouple (see Fig. 8(d)). The measuring errors (ΔT) comparing to the thermocouple were in the range from −1.37 °C and 1.83 °C (see Fig. 8(e)). Therefore, the GMR-based JNT can be used to measure temperature dynamically even when the GMR sensor experiences the varying external magnetic field.

V. Practical Demonstration of GMR-Based JNT

In order to demonstrate the feasibility of GMR-based JNT and verify that it can perform meaningful noise measurements in actual working conditions, a practical temperature

TABLE I
COMPARISON OF TEMPERATURE MEASUREMENT TECHNIQUES IN INDUSTRIAL APPLICATIONS [48]–[54]

Sensor type	Temperature range (°C)	Sensitivity	Output signal	Response time	Susceptibility to environment effects (*e.g.*, oxidation, corrosion, *etc.*)	Dual-parameter measurement
Thermocouple	−270 ~ 2300	±10 μV/°C	~10 mV	~100 ms	Susceptible	No
Resistance thermometer	−260 ~ 1064	0.1 Ω/°C	> 500 mV	approximately 1~100 s	Susceptible	No
Thermistors	−100 ~ 700	10 mV/K	> 100 mV	~1 s	Susceptible	No
Infrared thermometer	−40 ~ 2000	~0.1 °C	0 ~ 20 mA or 0 ~ 10 V	1 ms to 250 ms	Non-susceptible	No
Fiber optic probes	−200 ~ 2000	10 mV/°C	>10 mV	~1 s	Extremely Susceptible	Yes (Magnetic field and temperature)
Thermochromic liquid crystals	−40 ~ 283	±0.1°C	>10 mV	5 ms to seconds	Susceptible	No
Semiconductor devices	−55 ~ 150	±1%	>100 mV	100 ms ~ 1 s	Susceptible	No
GMR sensor (this work)	−40 ~ 150	~100 nV/√Hz/K	<1 μV/√Hz	A few seconds	Non-susceptible	Yes (Magnetic field and temperature)

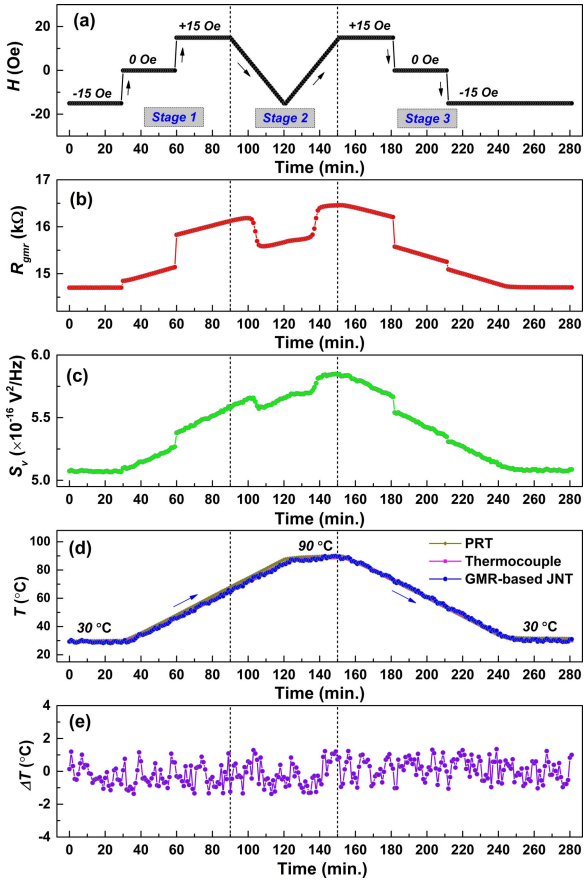

Fig. 8. Dynamic temperature measurement by the GMR-based JNT in a temperature cycle between 30 °C and 90 °C under varying magnetic field.

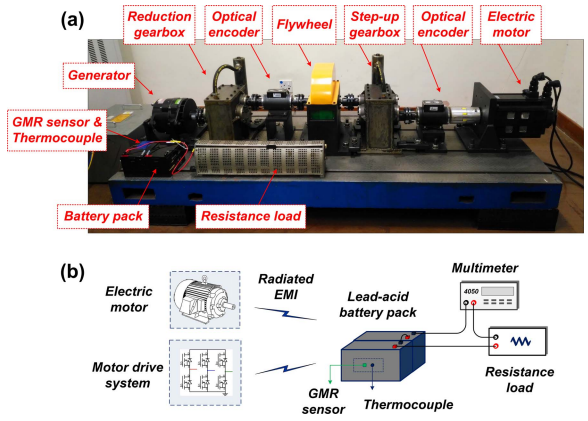

Fig. 9. (a) Photograph of the EV testbed for stimulating the actual EV environment. (b) Schematic of the practical demonstration of the GMR-based JNT.

measurement on an EV testbed was carried out. The EV testbed is composed of a 3-phase 5.5kW permanent magnet synchronous motor (PMSM), a high-speed flywheel, a step-up gearbox, a reduction gearbox, a permanent magnet synchronous generator (PMSG) and a battery pack (see Fig. 9(a)), which simulates the actual EV environment. The schematic of the practical demonstration of GMR-based JNT is shown in Fig. 9(b). Lead-acid batteries are being applied in EVs for vehicle propulsion [46], [47]. A battery pack composing of two rechargeable lead-acid batteries was applied to power a resistance load. The discharging current of the battery pack was monitored by a multimeter. A GMR sensor GF708 was placed on the surface of the battery pack. Similarly, a K-type thermocouple was placed in close proximity to the GMR sensor for providing a reference temperature. During the experiments, the PMSM of the EV testbed was operating through space vector control using an adjustable speed motor drive, and it rotated between the speed of approximately 100 rpm

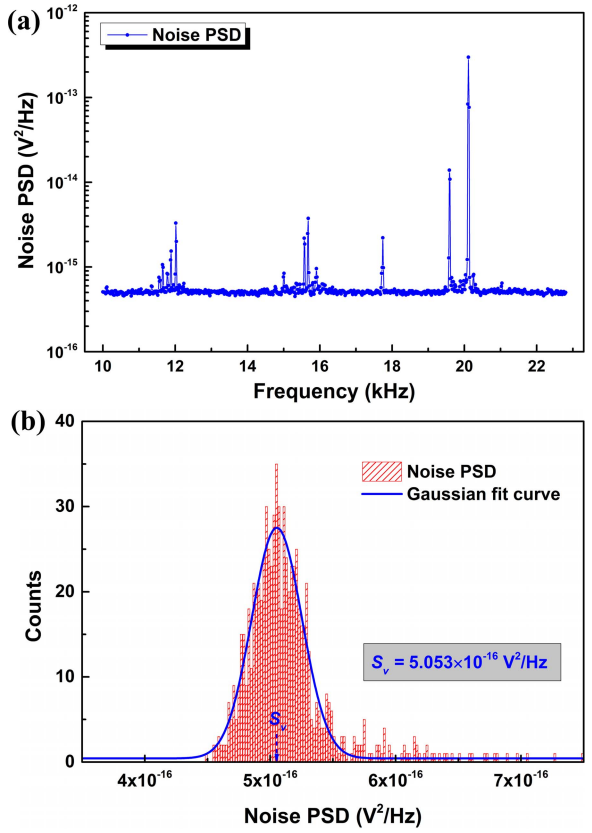

Fig. 10. (a) Power spectrum of the noise voltage in the observation bandwidth between 10 kHz and 22.8 kHz in an EV environment. (b) Gaussian fit of noise spectrum histograms to determine the averaged noise PSD value.

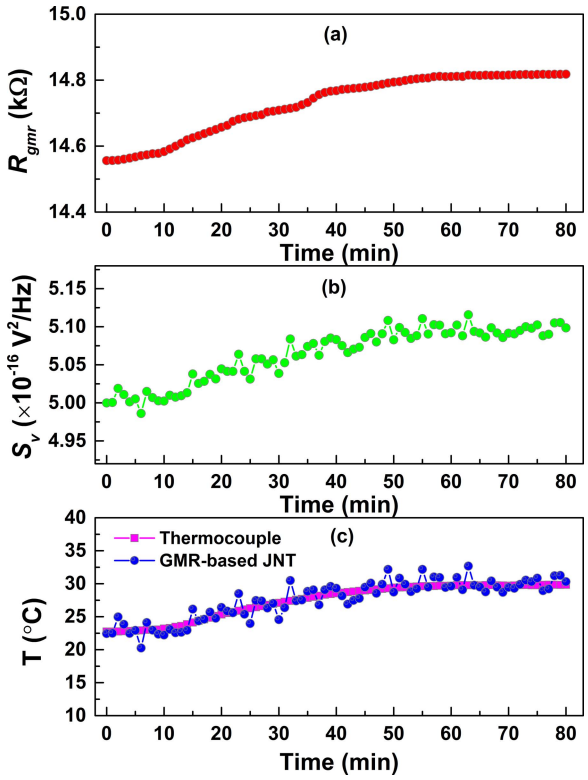

Fig. 11. Surface temperature measurement of EV battery pack during the discharging operation by the GMR-based JNT.

and 200 rpm. In the meanwhile, the motor was coupled with the high-speed flywheel and generator to adjust the load level during the temperature measurements.

There exist several noise sources (e.g. EMIs) in this EV testbed including electric motor drives and switching power supplies, etc. Fig. 10(a) shows the typical noise spectrum after 1000 times average in the frequency bandwidth between 10 kHz and 22.8 kHz. It can be observed there exist a few sharp spikes due to background EMI in the noise spectrum, but these narrowband sparks have a short frequency range. Though these few sharp sparks exhibit large noise PSD values, they are not representative of the average PSD for the noise spectrum in this frequency range because they have very few occurrence in the noise spectrum histogram. By the mean value of the Gaussian fit of the obtained histogram as illustrated in Fig. 10(b), the estimation of the noise PSD value was not sensitive to the effect of unwanted sharp EMI spikes. Although the broadband EMI noises may occur in the noise spectrum in a practical operating environment of EV, the Gaussian fit can still operate when the bandwidth of broadband EMI does not excessively occupy (e.g. <50%) the observation bandwidth. This is because that the most-frequently occurred value in noise spectrum is chosen as the noise PSD value with the Gaussian fit method. In the extreme scenario where the broadband EMI noises overwhelmingly dominate in the noise spectrum, the JNT can have a pause until a more well-detectable noise spectrum is measured.

The surface temperature of battery pack increased slowly from approximately 22.7 °C to 30 °C during the discharging operation. The sensor resistance (R_{gmr}) and averaged noise PSD (S_v) varied according to the surface temperature change of the battery pack, as shown in Fig. 12 (a) and Fig. 12(b) respectively. The surface temperature of the battery pack measured by GMR-based JNT also matched with those obtained by the thermocouple (see Fig. 12(c)). The practical measuring errors were within the range from −2.67 °C to 3.08 °C. This measurement uncertainty was larger than the experimental results in Section IV, which may result from the existence of radiated noises sources in an EV environment. Yet the temperature measured by GMR-JNT can still match with the temperature measured by the thermocouple. Therefore, it demonstrated the feasibility and possibility of using the GMR-based JNT to dynamically measure the temperature for practical EV applications.

As a final remark, the main characteristics of the proposed GMR-based JNT are summarized in Table I and compared with other commonly used temperature measurement methods in industrial applications [48]–[54]. It is observed that the reported GMR-based JNT in this manuscript shows features of reasonably fast response, dual-parameter measurement operation, robustness in harsh environment as well as robustness relatively wide temperature measurement range. It should be noted that other GMR sensors, such as a spin-valve based current sensor introduced in [35], are also applicable for the GMR-based JNT, which can achieve the dual-function operation for measurements of electric current and temperature

using one sensor. This advantage will provide insights for the large-scale applications of GMR sensors combined with intelligent sensing technologies [55], [56], such as electric vehicle applications.

VI. Conclusion

In this paper, a novel Johnson-noise-based thermometry using a GMR sensor as a sensing resistor has been investigated in various situations with external magnetic fields applied. This GMR-based JNT was experimentally demonstrated under both changing magnetic field and changing temperature. The measured temperatures by a GMR sensor were compared to those measured by a K-type thermocouple. The experimental results showed good linearity response, high accuracy, and reliability of this GMR-based JNT in a wide temperature range from -40 °C to 150 °C. The proposed thermometry also demonstrated its practical application for measuring the surface temperature of a battery pack on an electric vehicle testbed.

This study is of great use for developing a multifunctional spintronic sensor which measures velocity, current as well as temperature in EV applications. In future work, an integrated circuit system to implement the GMR-based JNT will be designed by using quite standard electronic components, which will replace the laboratory grade instruments introduced in this paper and make the GMR-based JNT feasible for the actual EV applications. An ultra-low noise preamplifier circuit with an equivalent input noise as 3.1 $\text{nV}/\sqrt{\text{Hz}}$ (at 1 kHz) for noise measurement will be obtained by consisting of three cascaded gain stages. This preamplifier circuit is composed of a large-area JFET transistor pair as the first stage, an ultra-low noise precision operational amplifier (e.g. LT1028 from Linear Technology) as the second stage and four low-noise rail-to-rail amplifiers connected in parallel as the third stage, resulting in an overall gain of 60 dB. A 10 μA constant current source provided by a voltage reference, a precision operational amplifier and a current-scaling resistor will be applied for the resistance measurement of GMR sensor. A high-speed FPGA chip combined with ADC modules will carry out the signal processing for determination of noise PSD and finally calculate out the absolute temperature. This integrated circuit system will reduce the measuring time by enlarging the observation bandwidth of noise and also ensure much faster measurement of noise PSD and temperature. Hence, it will replace the signal analyzer, source-meter, pre-amplifier, and computer to miniaturize the measurement system. This simple, cost-effective solution can be used to implement this GMR-based JNT in actual EV applications. The related work will be reported in the near future.

References

[1] E. J. Cairns and P. Albertus, "Batteries for electric and hybrid-electric vehicles," *Annu. Rev. Chem. Biomol. Eng.*, vol. 1, pp. 299–320, Jul. 2010.

[2] Q. Wang, P. Ping, X. Zhao, G. Chu, J. Sun, and C. Chen, "Thermal runaway caused fire and explosion of lithium ion battery," *J. Power Sour.*, vol. 208, pp. 210–224, Jun. 2012.

[3] S. M. Rezvanizaniani, Z. Liu, Y. Chen, and J. Lee, "Review and recent advances in battery health monitoring and prognostics technologies for electric vehicle (EV) safety and mobility," *J. Power Sour.*, vol. 256, pp. 110–124, Jun. 2014.

[4] S. Senty, "Chapter 6: Motor Nameplates," in *Motor Control Fundamental*, 1st ed. Boston, MA, USA: Cengage, 2012.

[5] Pittman Motors. *Temperature Effects on Motor Performance*. Accessed: Jul. 2017. [Online]. Available: http://www.pittman-motors.com/

[6] M. S. K. Mutyala, J. Zhao, J. Li, H. Pan, C. Yuan, and X. Li, "*In-situ* temperature measurement in lithium ion battery by transferable flexible thin film thermocouples," *J. Power Sour.*, vol. 260, pp. 43–49, Aug. 2014.

[7] R. R. Richardson, P. T. Ireland, and D. A. Howey, "Battery internal temperature estimation by combined impedance and surface temperature measurement," *J. Power Sour.*, vol. 265, pp. 254–261, Nov. 2014.

[8] J. Fan *et al.*, "Thermal analysis of permanent magnet motor for the electric vehicle application considering driving duty cycle," *IEEE Trans. Magn.*, vol. 46, no. 6, pp. 2493–2496, Jun. 2010.

[9] A. Graf, M. Arndt, and G. Gerlach, "Seebeck's effect in micromachined thermopiles for infrared detection. A review," *Proc. Estonian Acad. Sci. Eng.*, vol. 13, no. 4, pp. 338–353, 2007.

[10] A. Steele *et al.*, "CCT-K2: Key comparison of capsule-type standard platinum resistance thermometers from 13.8 K to 273.16 K," *Metrologia*, vol. 39, no. 6, pp. 551–571, 2002.

[11] D. White *et al.*, "The status of Johnson noise thermometry," *Metrologia*, vol. 33, no. 4, pp. 325–335, 1996.

[12] G. Scandurra, G. Cannatà, and C. Ciofi, "Fast Johnson noise thermometry using a temperature dependent sensor," in *Proc. I2MTC*, Graz, Austria, May 2012, pp. 1870–1875.

[13] F. Edler and P. Seefeld, "Self-validating contact thermometry sensors for higher temperatures," *Meas. Sci. Technol.*, vol. 26, no. 1, p. 015102, 2014.

[14] J. Crossno, X. Liu, T. A. Ohki, P. Kim, and K. C. Fong, "Development of high frequency and wide bandwidth Johnson noise thermometry," *Appl. Phys. Lett.*, vol. 106, no. 2, p. 023121, 2015.

[15] T. Yamada, C. Urano, and M. Maezawa, "Demonstration of Johnson noise thermometry with all-superconducting quantum voltage noise source," *Appl. Phys. Lett.*, vol. 108, no. 4, p. 042605, 2016.

[16] S. Benz, D. R. White, J. Qu, H. Rogalla, and W. Tew, "Electronic measurement of the Boltzmann constant with a quantum-voltage-calibrated Johnson noise thermometer," *Comptes Rendus Phys.*, vol. 10, no. 9, pp. 849–858, 2009.

[17] R. Slatter, "Magnetoresistive sensors for high performance electric drives," in *Proc. EDPC*, Nuremberg, Germany, Oct. 2012, pp. 1–6.

[18] C. Giebeler, D. J. Adelerhof, A. E. T. Kuiper, J. B. A. van Zon, D. Oelgeschläger, and G. Schulz, "Robust GMR sensors for angle detection and rotation speed sensing," *Sens. Actuators A, Phys.*, vol. 91, nos. 1–2, pp. 16–20, 2001.

[19] C. P. O. Treutler, "Magnetic sensors for automotive applications," *Sens. Actuators A, Phys.*, vol. 91, nos. 1–2, pp. 2–6, Jun. 2001.

[20] C. S. Anoop and B. George, "New signal conditioning circuit for MR angle transducers with full-circle range," *IEEE Trans. Instrum. Meas.*, vol. 62, no. 5, pp. 1308–1317, May 2013.

[21] L. Hao, X. Yanliang, Z. Yun, and L. Yuandong, "Development of steering wheel angle sensor used for torque coordinating control of in-wheel motor driven electric vehicle," in *Proc. ICEMS*, Beijing, China, Aug. 2011, pp. 1–3.

[22] A. Patel and M. Ferdowsi, "Current sensing for automotive electronics-A survey," *IEEE Trans. Veh. Technol.*, vol. 58, no. 8, pp. 4108–4119, Aug. 2009.

[23] T. P. Bohn, R. D. Lorenz, and E. R. Olson, "Measurement of *in-situ* currents in a hybrid electric vehicle integrated power module using giant magnetoresistive sensors," in *Proc. IEEE Power Electron. Transport.*, Oct. 2004, pp. 55–59.

[24] T. J. Brauhn, M. Sheng, B. A. Dow, H. Nogawa, and R. D. Lorenz, "Module-integrated GMR-based current sensing for closed-loop control of a motor drive," *IEEE Trans. Ind. App.*, vol. 53, no. 1, pp. 222–231, Jan. 2017.

[25] F. Rothan, C. Condemine, B. Delaet, O. Redon, and A. Giraud, "A low power 16-channel fully integrated GMR-based current sensor," in *Proc. Conf. ESSCIRC*, Bordeaux, France, Sep. 2012, pp. 245–248.

[26] A. De Marcellis *et al.*, "Monolithic integration of GMR sensors for standard CMOS-IC current sensing," *Solid-State Electron.*, vol. 135, pp. 100–104, Sep. 2017.

[27] X. Yan *et al.*, "Lowly loaded carbon nanotubes induced high electrical conductivity and giant magnetoresistance in ethylene/1-octene copolymers," *Polymer*, vol. 103, pp. 315–327, Oct. 2016.

[28] J. Guo *et al.*, "Enhanced negative magnetoresistance with high sensitivity of polyaniline interfaced with nanotitania," *J. Electrochem. Soc.*, vol. 163, no. 8, pp. 664–671, 2016.

[29] H. Gu *et al.*, "Strengthened magnetoresistive epoxy nanocomposite papers derived from synergistic nanomagnetite-carbon nanofiber nanohybrids," *Adv. Mater.*, vol. 27, no. 40, pp. 6277–6282, 2015.
[30] K. Sun *et al.*, "Flexible polydimethylsiloxane/multi-walled carbon nanotubes membranous metacomposites with negative permittivity," *Polymer*, vol. 125, pp. 50–57, Sep. 2017.
[31] C. Reig, M.-D. Cubells-Beltrán, and D. R. Muñoz, "Magnetic field sensors based on giant magnetoresistance (GMR) technology: Applications in electrical current sensing," *Sensors*, vol. 9, no. 10, pp. 7919–7942, Oct. 2009.
[32] Z. Q. Lei, G. J. Li, W. F. Egelhoff, P. T. Lai, and P. W. T. Pong, "Review of noise sources in magnetic tunnel junction sensors," *IEEE Trans. Magn.*, vol. 47, no. 3, pp. 602–612, Mar. 2011, doi: 10.1109/TMAG.2010.2100814.
[33] D. White and E. Zimmermann, "Preamplifier limitations on the accuracy of Johnson noise thermometers," *Metrologia*, vol. 37, no. 1, p. 11, 2000.
[34] G. Xiao, "Magnetoresistive sensors based on magnetic tunneling junctions," in *Handbook of Spin Transport and Magnetism*, E. Tsymbal and I. Zutic, Eds. Boca Raton, FL, USA: Taylor & Francis, 2012.
[35] C. Reig, D. Ramırez, F. Silva, J. Bernardo, and P. Freitas, "Design, fabrication, and analysis of a spin-valve based current sensor," *Sens. Actuators A, Phys.*, vol. 115, no. 2, pp. 259–266, 2004.
[36] M. D. Cubells-Beltrán, C. Reig, D. R. Muñoz, S. de Freitas, and P. de Freitas, "Full Wheatstone bridge spin-valve based sensors for IC currents monitoring," *IEEE Sensors J.*, vol. 9, no. 12, pp. 1756–1762, Dec. 2009.
[37] C. Ye, Y. Huang, L. Udpa, S. Udpa, and A. Tamburrino, "Magnetoresistive sensor with magnetic balance measurement for inspection of defects under magnetically permeable fasteners," *IEEE Sensors J.*, vol. 16, no. 8, pp. 2331–2338, Apr. 2016.
[38] J. Xu *et al.*, "Detection of the concentration of $MnFe_2O_4$ magnetic microparticles using giant magnetoresistance sensors," *IEEE Trans. Magn.*, vol. 52, no. 4, pp. 1–4, Apr. 2016.
[39] L. Li, K. Y. Mak, C. W. Leung, S. M. Ng, Z. Q. Lei, and P. W. T. Pong, "Detection of 10-nm superparamagnetic iron oxide nanoparticles using exchange-biased GMR sensors in Wheatstone bridge," *IEEE Trans. Magn.*, vol. 49, no. 7, pp. 4056–4059, Jul. 2013.
[40] *GF708 MagnetoResistive Magnetic Field Sensor*. Accessed: Jul. 2017. [Online]. Available: http://www.sensitec.com/
[41] P. P. Freitas *et al.*, "Optimization and integration of magnetoresistive sensors," *Spin*, vol. 1, no. 1, pp. 71–91, 2011.
[42] P. Thounthong, S. Raël, and B. Davat, "Control strategy of fuel cell/supercapacitors hybrid power sources for electric vehicle," *J. Power Sour.*, vol. 158, no. 1, pp. 806–814, 2006.
[43] T. Arakawa *et al.*, "Sub-Poissonian shot noise in CoFeB/MgO/CoFeB-based magnetic tunneling junctions," *Appl. Phys. Lett.*, vol. 98, no. 20, p. 202103, 2011.
[44] R. Cron, M. Goffman, D. Esteve, and C. Urbina, "Multiple-charge-quanta shot noise in superconducting atomic contacts," *Phys. Rev. Lett.*, vol. 86, no. 18, p. 4104, 2001.
[45] K. Sekiguchi *et al.*, "Observation of full shot noise in CoFeB/MgO/CoFeB-based magnetic tunneling junctions," *Appl. Phys. Lett.*, vol. 96, no. 25, p. 252504, 2010.
[46] V. H. Johnson, "Battery performance models in ADVISOR," *J. Power Sour.*, vol. 110, no. 2, pp. 321–329, 2002.
[47] A. Khaligh and Z. Li, "Battery, ultracapacitor, fuel cell, and hybrid energy storage systems for electric, hybrid electric, fuel cell, and plug-in hybrid electric vehicles: State of the art," *IEEE Trans. Veh. Technol.*, vol. 59, no. 6, pp. 2806–2814, Jul. 2010.
[48] P. Childs, J. Greenwood, and C. Long, "Review of temperature measurement," *Rev. Sci. Instrum.*, vol. 71, no. 8, pp. 2959–2978, 2000.
[49] Y.-G. Kim, I. Yang, S. Y. Kwon, and K. S. Gam, "Features of Co/C and Ni/C eutectic transitions for use in thermocouple thermometry," *Metrologia*, vol. 43, no. 1, p. 67, 2005.
[50] F. K. Meyer and A. E. Merbach, "Temperature measurement under high pressure using commercial platinum resistors," *J. Phys. E*, vol. 12, no. 3, p. 185, 1979.
[51] C. A. James, A. J. Richardson, P. W. Watt, and N. S. Maxwell, "Reliability and validity of skin temperature measurement by telemetry thermistors and a thermal camera during exercise in the heat," *J. Thermal Biol.*, vol. 45, pp. 141–149, Oct. 2014.
[52] P. Ireland and T. Jones, "The response time of a surface thermometer employing encapsulated thermochromic liquid crystals," *J. Phys. E, Sci. Instrum.*, vol. 20, no. 10, p. 1195, 1987.
[53] X.-G. Li *et al.*, "Measurement of magnetic field and temperature based on fiber-optic composite interferometer," *IEEE Trans. Instrum. Meas.*, vol. 66, no. 7, pp. 1906–1911, Jul. 2017.
[54] A. Szmyrka-Grzebyk and L. Lipiński, "Linear diode thermometer in the 4-300 K temperature range," *Cryogenics*, vol. 35, no. 4, pp. 281–284, 1995.
[55] C. Alippi, "A unique timely moment for embedding intelligence in applications," *CAAI Trans. Intell. Technol.*, vol. 1, pp. 1–3, Jun. 2016.
[56] S. Padhy and S. Panda, "A hybrid stochastic fractal search and pattern search technique based cascade PI-PD controller for automatic generation control of multi-source power systems in presence of plug in electric vehicles," *CAAI Trans. Intell. Technol.*, vol. 2, no. 1, pp. 12–25, 2017.

Xuyang Liu (S'16) received the B.Eng. degree from the University of Electronic Science and Technology of China, Chengdu, China, in 2015. He is currently pursuing the Ph.D. degree with the Department of Electrical and Electronic Engineering, University of Hong Kong, Hong Kong. His current research interests include nondestructive testing, advanced sensing technologies, applications of magnetoresistive magnetic field sensors in electric vehicles, and wireless power transfer.

Chao Zheng received the B.S. degree in applied physics from the Zhejiang University of Technology, Zhejiang, China. He is currently pursuing the Ph.D. degree with the Department of Electrical and Electronic Engineering, University of Hong Kong, Hong Kong. Since 2013, he has been carrying out experimental and theoretical research of spin transportation and low-frequency noise in magnetoresistive sensors. He is currently a taskforce member of the roadmap for magnetoresistive sensors. His research interests include development of highly-sensitive magnetic tunnel junction sensors for ultralow-field-sensing applications, fundamental study of magnetic low-frequency noise in magnetic tunnel junction sensors, and magnetic thin films.

Chunhua Liu (M'10–SM'14) received the B.Eng. and M.Eng. degrees from the Department of Automatic Control, Beijing Institute of Technology, China, in 2002 and 2005, respectively, and the Ph.D. degree from the Department of Electrical and Electronic Engineering, University of Hong Kong, Hong Kong, in 2009. He currently serves as an Assistant Professor with the School of Energy and Environment, City University of Hong Kong, Hong Kong.

His research interests are in electrical energy and power technology, including electric machines and drives, electric vehicles, electric robotics and ships, renewable energy and microgrid, and wireless power transfer. In these areas, he has published over 130 refereed papers.

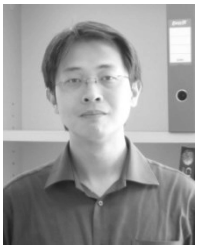

Philip W. T. Pong (SM'13) received the Ph.D. degree in engineering from the University of Cambridge in 2005. He was a Post-Doctoral Researcher with the Magnetic Materials Group, National Institute of Standards and Technology for three years. In 2008, he joined the University of Hong Kong (HKU) Engineering Faculty, where he is now an Associate Professor working on magnetoresistive sensors and their application in smart grid and smart living. He is also a Physicist and Electrical Engineer working on magnetoresistive magnetic field sensors and smart grid with the Department of Electrical and Electronic Engineering, HKU.